Optical Engineering

OpticalEngineering.SPIEDigitalLibrary.org

Noncontact on-machine measurement system based on capacitive displacement sensors for single-point diamond turning

Xingchang Li
Zhiyu Zhang
Haifei Hu
Yingjie Li
Ling Xiong
Xuejun Zhang
Jiwang Yan

SPIE.

Xingchang Li, Zhiyu Zhang, Haifei Hu, Yingjie Li, Ling Xiong, Xuejun Zhang, Jiwang Yan, "Noncontact on-machine measurement system based on capacitive displacement sensors for single-point diamond turning," *Opt. Eng.* **57**(4), 044105 (2018), doi: 10.1117/1.OE.57.4.044105.

Optical Engineering 57(4), 044105 (April 2018)

Noncontact on-machine measurement system based on capacitive displacement sensors for single-point diamond turning

Xingchang Li,[a,b] Zhiyu Zhang,[a,*] Haifei Hu,[a,c] Yingjie Li,[a] Ling Xiong,[a] Xuejun Zhang,[a] and Jiwang Yan[d]
[a]Chinese Academy of Sciences, Key Laboratory of Optical System Advanced Manufacturing Technology, Changchun Institute of Optics, Fine Mechanics and Physics, Changchun, Jilin, China
[b]University of Chinese Academy of Sciences, Beijing, China
[c]Jilin University, School of Mechanical Science and Engineering, Changchun, Jilin, China
[d]Keio University, Department of Mechanical Engineering, Yokohama, Japan

Abstract. On-machine measurements can improve the form accuracy of optical surfaces in single-point diamond turning applications; however, commercially available linear variable differential transformer sensors are inaccurate and can potentially scratch the surface. We present an on-machine measurement system based on capacitive displacement sensors for high-precision optical surfaces. In the proposed system, a position-trigger method of measurement was developed to ensure strict correspondence between the measurement points and the measurement data with no intervening time-delay. In addition, a double-sensor measurement was proposed to reduce the electric signal noise during spindle rotation. Using the proposed system, the repeatability of 80-nm peak-to-valley (PV) and 8-nm root-mean-square (RMS) was achieved through analyzing four successive measurement results. The accuracy of 109-nm PV and 14-nm RMS was obtained by comparing with the interferometer measurement result. An aluminum spherical mirror with a diameter of 300 mm was fabricated, and the resulting measured form error after one compensation cut was decreased to 254 nm in PV and 52 nm in RMS. These results confirm that the measurements of the surface form errors were successfully used to modify the cutting tool path during the compensation cut, thereby ensuring that the diamond turning process was more deterministic. In addition, the results show that the noise level was significantly reduced with the reference sensor even under a high rotational speed. [DOI: 10.1117/1.OE.57.4.044105]

Keywords: single-point diamond turning; capacitive displacement sensor; noncontact measurement; high efficiency; compensation.

Paper 171736 received Nov. 8, 2017; accepted for publication Apr. 3, 2018; published online Apr. 20, 2018.

1 Introduction

Over the past several decades, great progress has been made in single-point diamond turning (SPDT) technology, especially in terms of the surface roughness and form accuracy.[1–6] SPDT technology can potentially finish a surface profile to submicron accuracy with nanometer surface roughness in only one cut, and thus offers significant advantages over other processes, such as milling, lapping, and polishing, as those require multiple steps to achieve similar levels of surface roughness and form accuracy.

In recent years, aluminum 6061 has come to be considered as a competitive material for manufacturing reflective mirrors for astronomical applications.[7,8] Compared with some hard and brittle materials such as high-phosphorous nickel and germanium, aluminum 6061 is soft and ductile and can easily be processed with the SPDT technology. When aluminum 6061 is machined with the surface accuracy of diamond turning, the resulting mirrors can satisfy the application requirements for infrared components; however, the surface accuracy is not sufficient for visible light components. To improve the low-frequency form accuracy, compensation cuttings are always required to recut the surface. However, before recutting, it is preferred that the surface profile be first measured by an on-machine metrology system.

There are several methods of realizing on-machine measurements. A touching probe, i.e., the so-called linear variable differential transformer (LVDT), is always installed on a commercial diamond turning machine. However, the touching method has low accuracy that can potentially scratch the soft surface of the aluminum 6061. Other methods include laser and chromatic confocal probes, which are noncontact and nondestructive methods for surface measurement. However, laser beams are susceptible to the presence of residual coolant fluid or cutting debris on the testing surface.

In contrast to the above-mentioned methods of measurement, we propose a compact testing system using capacitive sensors, which are noncontact devices that are capable of high-resolution measurements based on changes in position. In our previous work, we demonstrated that such sensors are well suited for measurement applications as they are simple, convenient, and reliable. However, it was also found that the performance of capacitive sensors was significantly influenced by environmental conditions, such as the ambient temperature and vibrations from the base of the machine.[9]

*Address all correspondence to: Zhiyu Zhang, E-mail: zhangzhiyu@ciomp.ac.cn

0091-3286/2018/$25.00

In our previous work, through comparing with the result of interferometer measurement, the measurement accuracy for low-order surface form error using the capacitive sensor on a general-precision machining center was found to be 0.278 μm peak-to-valley (PV) and 0.048 μm root-mean-square (RMS),[9] which is significantly worse than the nominal resolution of the selected capacitive sensor. The measurement performance of a capacitive sensor system on an ultraprecision machine tool has not reported. With the application of antivibration techniques and stable temperature control, it should be possible to create a more stable and accurate measurement system using capacitive sensors. Therefore, in this work we describe the development and evaluation of a metrology system using capacitive sensors on an ultraprecision machine tool.

2 Metrology

2.1 *Measurement System*

A schematic diagram of the capacitive displacement sensor and corresponding electric field distribution is shown in Fig. 1. As shown in the figure, the sensor is cylindrical and the bottom circular planar surface is the effective working surface for measurements. The interior structure of the sensor consists of a ground, screening, and measuring electrodes. The theory of a capacitive sensor is based on the principle of parallel plate capacitance as per the following equation:

$$X_c = \frac{d}{j\omega\varepsilon_0\varepsilon_r S}, \tag{1}$$

where X_c is the capacitive reactance, ω is the angular velocity of the alternating current, ε_0 is the vacuum permittivity, ε_r is the relative permittivity, S is the measured area, and d is the distance from the measured area to the working surface of the sensor, respectively. The capacitive reactance X_c is proportional to d during the measurement process as long as the other variables in Eq. (1) remain unchanged. The capacitive sensor translates the capacitance information into an analog signal output, and then the measurement system translates that into distance information.

The end of the cylindrical capacitive sensor is circular to measure the positional changes. The sampling area on a measured surface is usually in the tens of square millimeters, which is much larger than the micron-order sampling area of a focused laser beam and LVDT probe. The much larger sampling area of a capacitive sensor can be used to average the local high-frequency influence on the PV value, which

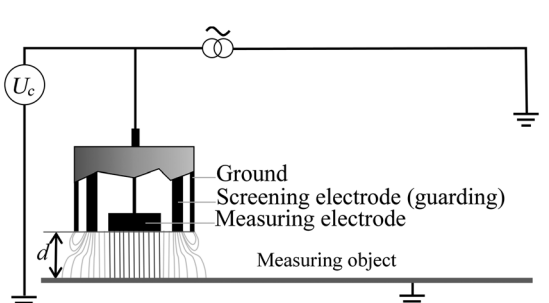

Fig. 1 Schematic diagram of the capacitive displacement sensor.

can significantly decrease the influence of residual cutting chips or debris on the measurement results.

The types of objects that can be measured with a capacitive sensor include electrical conductors and semiconductors, e.g., silicon and silicon carbide, although the corresponding electric field distributions are not shown here.[10]

A schematic of the measurement system when installed on an ultraprecision machine tool is shown in Fig. 2(a). The machine tool is composed of an air bearing spindle with a vacuum chuck, two perpendicular hydrostatic linear tables (X- and Z-axes), and a hydrostatic rotary table (B-axis). A capacitive sensor is attached to an adjustable fixture mounted on the B-axis table. A high-resolution data acquisition system is used to record the changes of position, as shown in Fig. 2(b). The specifications of the measurement system are shown in Table 1.

2.2 *Sensor Alignment*

Before initiating a measurement, the coordinate system of the capacitive sensor should be coincident with the workpiece coordinate system. To start, fine adjustments should be made to the sensor height, and the rotation radius of the sensor should be measured, as shown in Figs. 3(a) and 3(b), respectively. The height-direction alignment of the sensor is based on the calibrated diamond tool height plus the radius of the sensor. The total height is the height of the peak generatrix of the sensor. In the experiments in this paper, the measurement of the diamond tool height, geometric radius of the sensor, adjustment of the height of the sensor, as well as the measurement of the rotation radius of the sensor, were all conducted by means of a commercial laser tracker. The procedure is as follows: initially, the rotation axis and a horizontal base plane could be determined through rotating the B-axis table. Afterward, the radius of the working surface and the location of the cylinder center axis could be obtained by measuring its cylindrical surface. Subsequently, the location of the working surface could be acquired through touching the tracker ball to it. Thus, the intersection point of the cylinder center axis with the working surface of the sensor was the reference point of the sensor position. The distance from the reference point to the rotation axis of the B-axis was the rotation radius of the sensor. The height from the reference point to the horizontal base plane could be regarded as the height of the sensor. In addition, the tool height to the horizontal base plane could be obtained by touching the tracker ball to the rake face of the diamond tool. The sensor height could be accurately obtained by adjusting the height of the reference point to the height of the diamond tool.

Due to the noncontact measurement feature, the sensor can be installed as a fixed tool for on-machine measurement that only requires periodic calibration after the initial adjustment procedure has been completed.

Once the above adjustments are complete, the sensor can be aligned to the spindle rotation center along the X-axis direction by scanning along the diameter of a trial-machined part on the spindle. It is known that a part after diamond cutting always has a rotational symmetric form error. Therefore, the symmetric center of the measured profile after diameter scanning along the X-direction should be the position of the spindle rotation center. A schematic of the diameter scanning method and another showing the obtained profile are shown

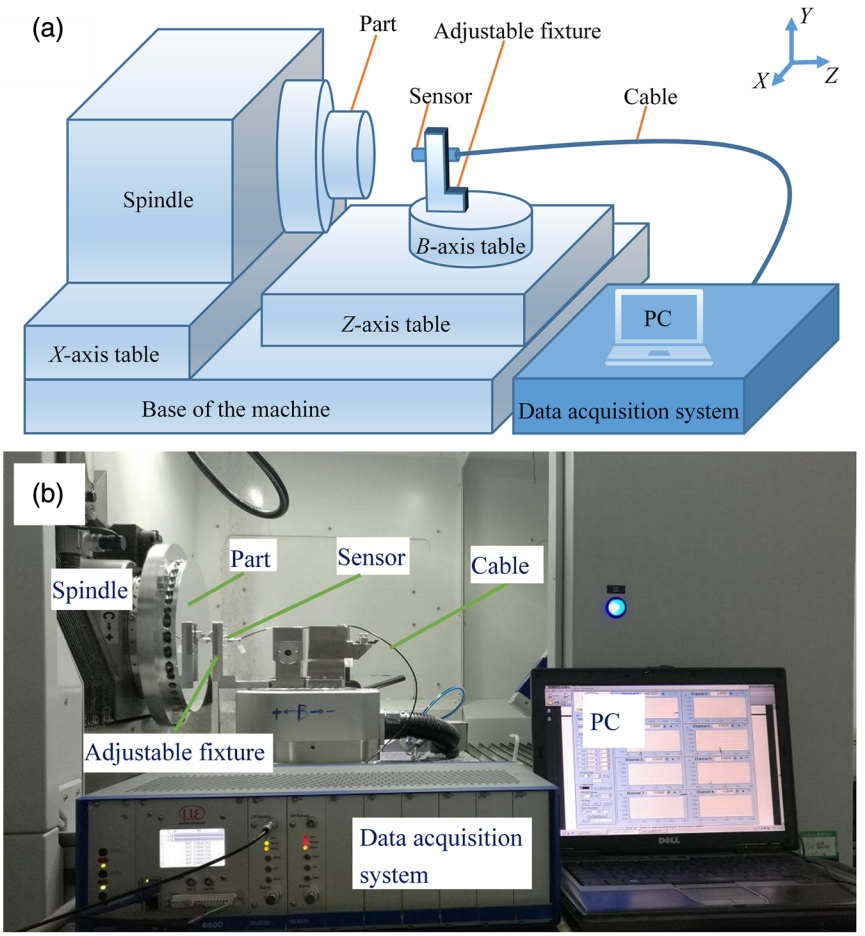

Fig. 2 Measurement system based on an ultraprecision machine tool (a) schematic diagram of the setup and (b) an image of the setup.

Table 1 Specifications of the measurement system.

Items	Parameters
Measurement range (μm)	1000
Static resolution (nm)	0.75
Dynamic resolution (nm)	9
Typical linearity of full range (μm)	0.25
Maximum sampling frequency (kHz)	8.5
Diameter of outer cylinder (mm)	10
Diameter of effective working area (mm)	5.7

in Fig. 4. The results shown in Fig. 4(b) illustrate that by following the proposed diameter scanning method, it is possible to accomplish the alignment of the sensor with the rotational center of the spindle in the X-axis direction.

2.3 *Elimination of Nonlinear Errors*

Compared with laser displacement sensors, the capacitive displacement sensor achieves a higher resolution at the subnanometer level with improved stability. However, the problem of nonlinearity, which is a characteristic of this type of sensor, cannot be ignored in ultraprecision measurements.

2.3.1 *Linearity deviation*

In our previous work, the linearity deviation of the capacitive sensor was investigated and the deviation curve was found to be very similar to a sinusoidal wave in the measurement distance from 100 to 1000 μm, as shown in Fig. 5.[9] To realize linear measurement, the measurement distance should be set at the region with the minimum gradient in Fig. 5, which in this case is near to the measurement distance of 330 or 850 μm, where the linearity deviation can be considered to be constant in a small measurement range. In this paper, the initial measurement distance was selected to be near 850 μm. It should be noted that the typical form error of diamond-turned surfaces is within 10 μm. The linear deviation belonging to the corresponding region within 10 μm around 850 μm was sufficiently consistent and was, therefore, considered to have good linearity.

2.3.2 *Tilt-induced nonlinearity*

The misalignment of the working surface of the sensor with the measured surface of the workpiece can produce nonlinear

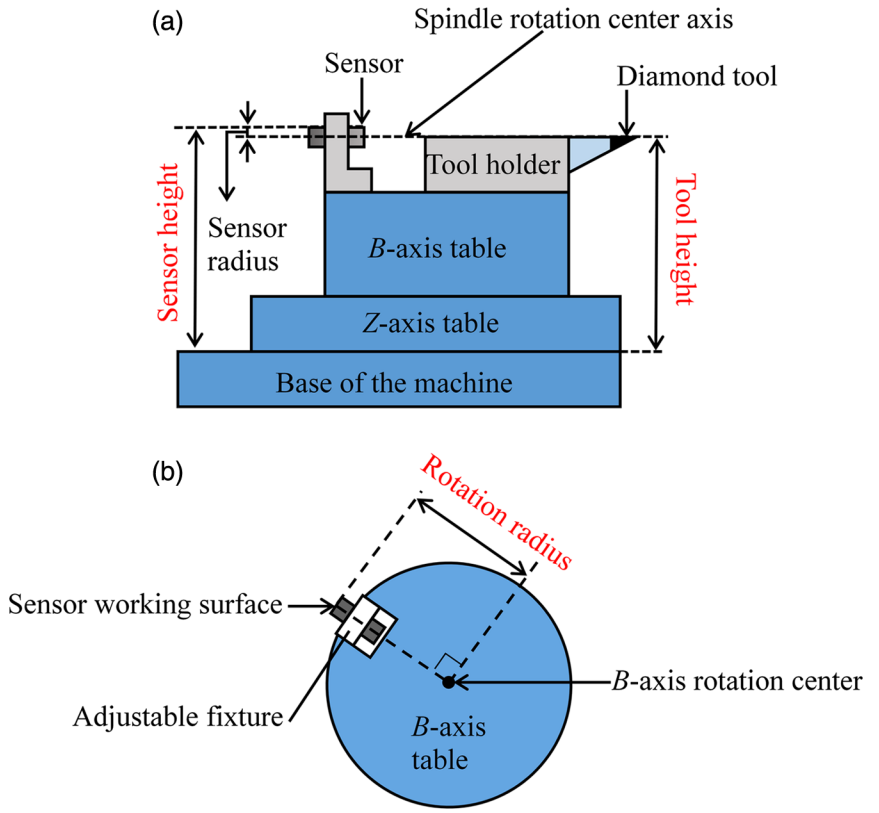

Fig. 3 Schematic of (a) the sensor height and (b) the radius of rotation.

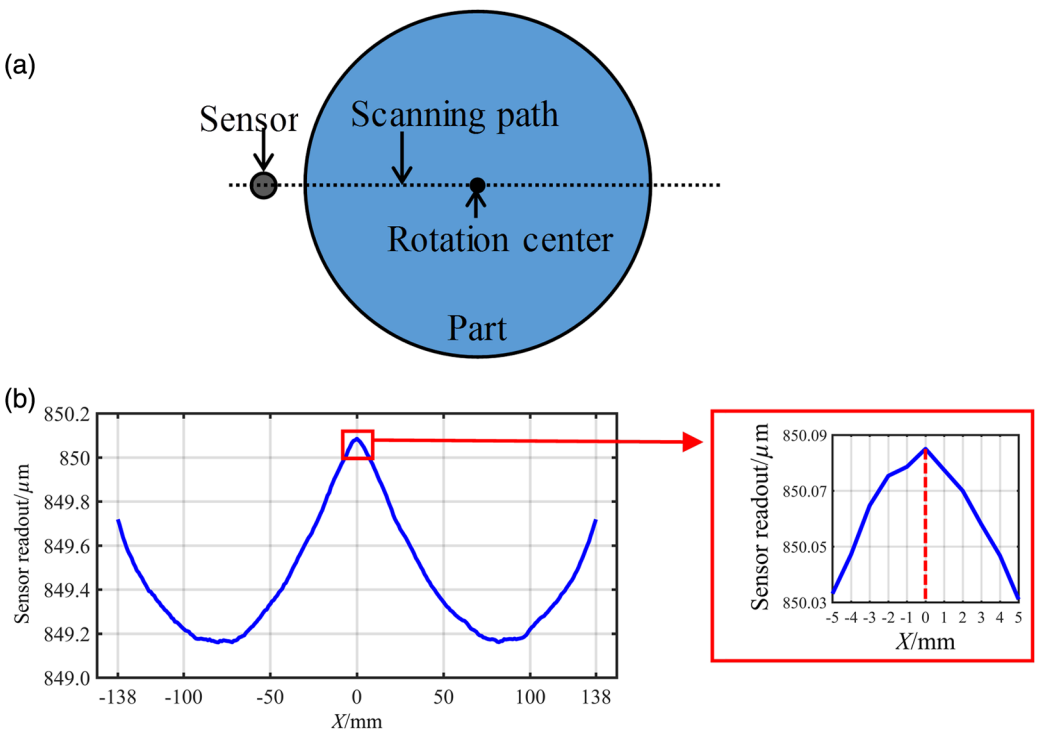

Fig. 4 (a) Schematic diagram showing the setup used to scan the diameter and (b) the profile obtained by scanning the diameter.

measurement results. In an ideal situation, the working surface of the sensor and the measured surface of the workpiece should be perfectly parallel; however, this is impossible in practical situations, as shown in Fig. 6. Suppose that θ is the tilt angle between the sensor and the measured surface and R is the radius of the effective working area. Then, the absolute measured error (ME) between the measurement result d_{meas} and the measurement distance d_{real} can be derived as

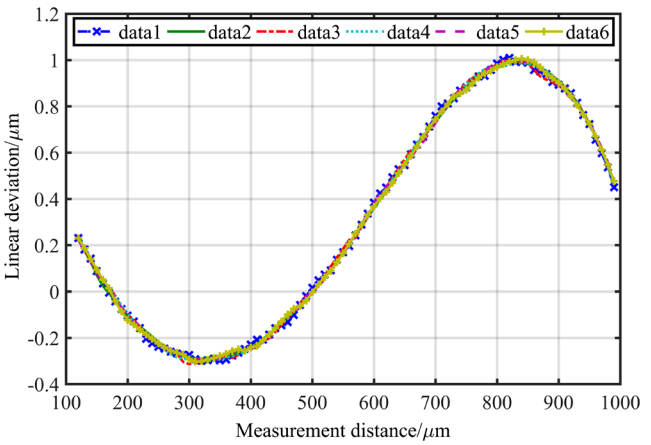

Fig. 5 Results of calibrating the linear deviation.

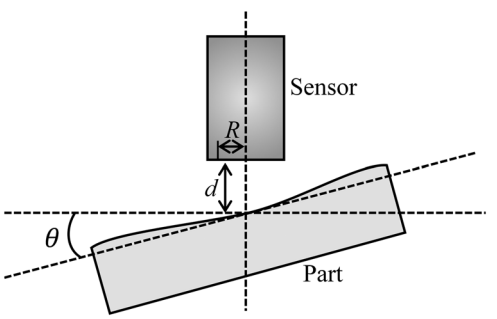

Fig. 6 Illustration of a measurement with a tilt angle.

$$d_{\text{meas}} = \frac{d_{\text{real}}}{2}\left[1 + \sqrt{1 - \left(\frac{R\tan\theta}{d_{\text{real}}}\right)^2}\right], \tag{2}$$

$$\text{ME} = d_{\text{meas}} - d_{\text{real}}. \tag{3}$$

If θ is 0.1 deg, then the relationship between ME and d_{real} is as shown in Fig. 7. According to Eqs. (2) and (3), the absolute measurement error can be calculated to be -0.0073 μm at a measurement distance of 850 μm. Moreover, it is reasonable to consider the measurement characteristic as linear within a distance change around 10 μm.

Ideally, it is important to maintain the same tilt angle for each measurement point so that the tool path of the single-point machining can be used as the sensor path while making measurements; however, the initial measurement distance from the sensor to the target mirror (set as 850 μm) must be subtracted from the radius of the tool path. By inserting feeler gages with a thickness of 10 μm between the spindle surface and the sensor to check the tilt interval, the tilt angle can be adjusted to within 0.1 deg. The tilt angle can be calculated as follows:

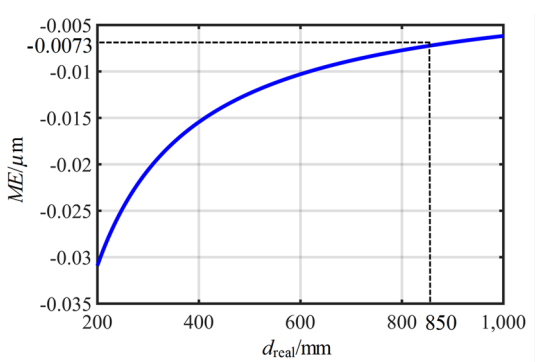

Fig. 7 Relationship between ME and d_{real} when the tilt angle is 0.1 deg.

$$\theta \approx \frac{10\ \mu\text{m}}{\text{D}}, \tag{4}$$

where D is the geometric diameter of the sensor.

The procedure for measuring a curved surface is shown in Fig. 8. After adjusting the tilt angle, the sensor should be rotated on the B-axis table to maintain the initial tilt angle unchanged during the measurement. Meanwhile, the positions of the X- and Z-axes tables should also be synchronously adjusted so that the form error in the radial direction can be precisely measured.

2.3.3 *Linearity correction*

To correct the linearity errors caused by the above-mentioned factors, an end-point reference calibration was carried out based on the initial measurement results of the surface profile. The end-point reference refers to the definition of straightness for linear axes on machine tools.[11] After the initial measurement, the maximum value $d_{\max}$ and minimum value $d_{\min}$ of the surface profile were obtained. The absolute value of the difference between $d_{\max}$ and $d_{\min}$ was defined as the length of the calibration section Δd_{cali}, as shown in Fig. 9 (units in microns), and Z_0 denotes the measurement position where the sensor readout was 850 μm. The Z-axis table was reciprocated three times between the end points of the calibration section, resulting in six readout changes from the sensor. The mean absolute value of the sensor readout changes was Δd_{mean}.

The relative measurement error in percentage (RME) can be computed using Eq. (5) and the measurement result can be linearly corrected using Eq. (6)

$$\text{RME} = \frac{\Delta d_{\text{mean}} - \Delta d_{\text{cali}}}{\Delta d_{\text{cali}}} \times 100\%, \tag{5}$$

$$d_{\text{corr}} = \frac{d_{\text{meas}}}{(1 + \text{RME})}, \tag{6}$$

where d_{corr} is the result after correction and d_{meas} is the measurement result. The length of the calibration section Δd_{cali} was found to be 0.969 μm, which was obtained from the difference of the measured $d_{\max}$ 850.243 μm and $d_{\min}$ 849.274 μm. The six readout changes during the course of three reciprocation cycles are shown in Table 2. The RME was calculated to be -0.221% using Eq. (5). Note that the initial results of the surface measurement described in Sec. 4.1 were corrected using Eq. (6). In view of the measurement principle of capacitive sensor, especially for aspheres and freeforms, the curvature difference across the aperture may influence the measurement result.

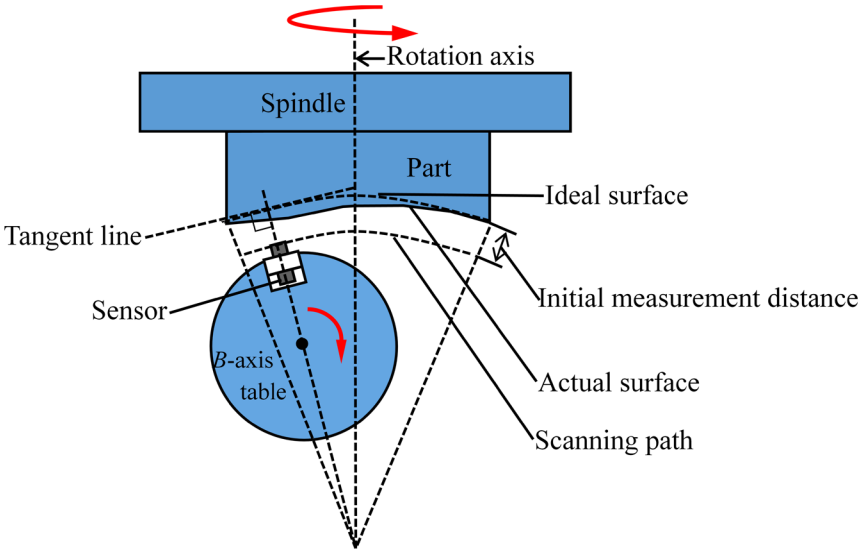

Fig. 8 Schematic diagram of the measurement scanning path.

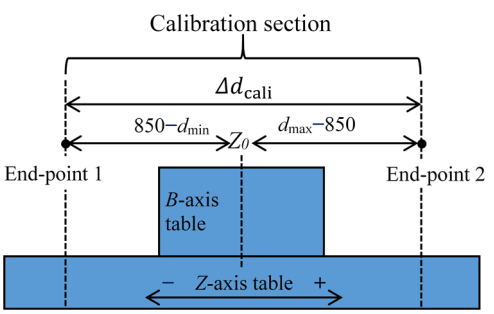

Fig. 9 Diagram showing the end-point reference correction method.

Table 2 Readout changes during linearity calibration.

No.	Readout changes (μm)
1	0.961
2	–0.974
3	0.970
4	–0.966
5	0.970
6	–0.958
Δd_{mean}	0.967

3 Experiment

To examine the repeatability and accuracy of the capacitive sensor system, an aluminum 6061 spherical mirror with a curvature radius of 630.75 mm and an aperture diameter of 262 mm was fabricated. The surface form error was measured by the on-machine capacitive sensor and off-machine interferometer as shown in Figs. 10(a) and 10(b), respectively.

Afterward, an aluminum 6061 mirror with an aperture diameter of 300 mm was fabricated. An on-machine measurement and compensation cutting experiment were carried out with the proposed method based on the capacitive sensor. The surface of the mirror was spherical with a curvature radius of 12.337 m, which could not be precisely measured by the interferometer due to lack of a reference sphere with such a large F number (the ratio of curvature radius to mirror aperture). The body of the mirror employed a patented lightweighted structure.[12]

3.1 *Position-Trigger Method of Measurement*

To realize full-aperture measurements, the data acquisition system recording the sensor readout must be synchronized with the current measurement coordinates. Therefore, a position-trigger method of measurement was developed to strictly correlate the measurement position with the current coordinates. When the measurement program appends the trigger codes at the end of each coordinate point to be measured, a rising edge signal is sent out to the data acquisition system. This instructs the data acquisition system to collect the measurement data at each coordinate point. The capacitive sensor supports a high sampling rate, which guarantees that the measurement points correspond exactly with the measured X- and Z-coordinates without any intervening time-delay. This configuration enables the measurement of a full-aperture surface to be completed in a very short time, and the overall measurement process is much more efficient than that used in the contact LVDT method.

The projection pattern of the measurement path in the $X-Y$ plane is shown in Fig. 11. The measurement process is very similar to the cutting process, and the measurement program has a similar complexity to that of a single-point cutting tool path. Using a scanning path in combination with the developed position-trigger method of measurement, the measurement of the surface form error is extremely efficient. During sampling, both the angle-increment between two adjacent points along the spiral path and the X-direction feedrate between each revolution were kept in constant.

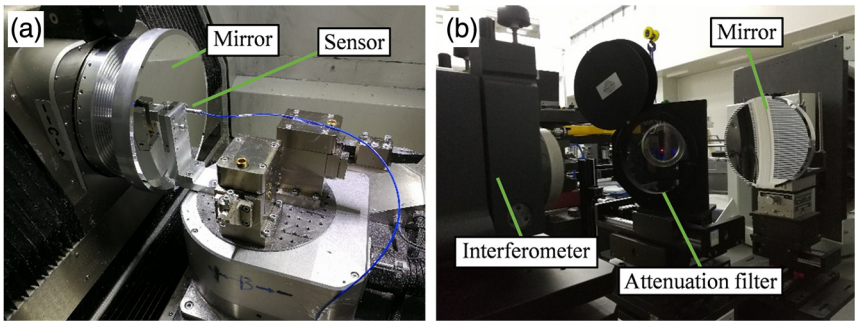

Fig. 10 Measurement processes (a) the on-machine measurement and (b) the off-machine interferometer measurement.

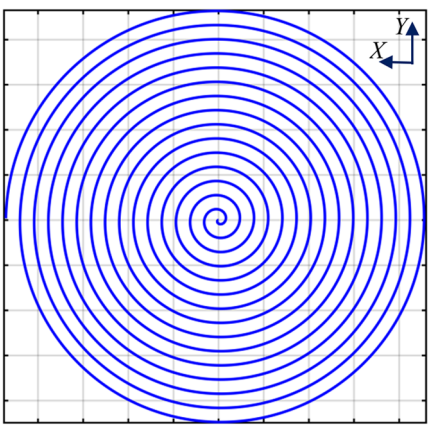

Fig. 11 Projection of the measurement path pattern in the $X - Y$ plane.

3.2 *Noise Elimination*

During the experiments, it was found that the collected data contained a large amount of white noise when the measured workpiece was rotated at high speed, whereas the noise was not present when the spindle was not rotating. The source of this noise was thought to be caused by the induced potential changes due to the rotation of the spindle. To eliminate the noise, a double-sensor measurement was proposed. As shown in Fig. 12, the measurement sensor was mounted on a B-axis table together with a reference sensor mounted on the spindle. As the electric noise was introduced by the induction of the potential changes on the measured surface, it can be counteracted by subtracting one readout from the other. Note that the double-sensor method will eliminate not only the induced noise, but also the influence of temperature changes during long-duration measurements.

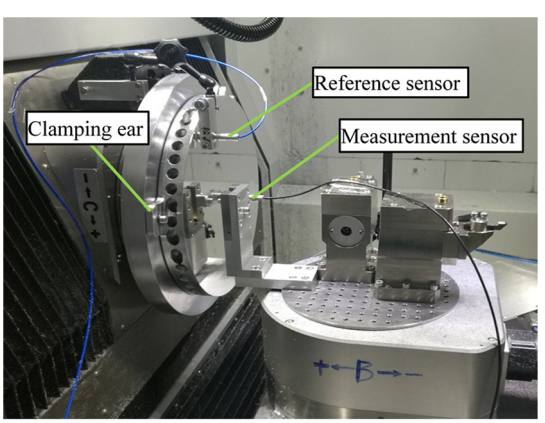

Fig. 12 Image showing the double-sensor measurement system.

4 Results and Discussion

4.1 *Examination of Repeatability and Accuracy*

On-machine measurements of the mirror with 630.75-mm curvature radius were successively carried out four times. The rotational speed of the spindle was set to 20 rpm and the sensor sampling frequency was set to 50 Hz. The angle-increment was 12 deg and the X-direction feedrate was 1 mm per revolution. Figure 13 shows the obtained results. Because of the relatively large diameter of the capacitive sensor, the measured aperture of this mirror was actually 246 mm, 93.9% of full aperture. A capacitive sensor with much smaller diameter can increase the measured aperture much closer to full aperture. In addition, the decrease in the sensor diameter will benefit the measurement of surfaces with varying curvatures.

To analyze the repeatability of the measurement, the results of the four measurements are averaged as shown in Fig. 14. Subtractions of the four measurement results to the average result are shown in Fig. 15, corresponding to the arrangement order in Fig. 13.

As shown in Fig. 15, the mean value of the deviations from the four measurement results to their average result is 0.080-μm PV and 0.008-μm RMS, which is considered as the repeatability in the measurement.

The interferometer measurement result within 246-mm aperture is shown in Fig. 16. A subtraction from the average result in Fig. 14 to the interferometer measurement result is shown in Fig. 17. The difference between the two results is 0.109-μm PV and 0.014-μm RMS, which is considered as the accuracy in the measurement.

It is clearly shown that the ring pattern, which was introduced by the diamond tool feed, becomes much more obvious in Fig. 17 than that in Fig. 16. That is because the low frequency form error obtained by the capacitive sensor was fairly subtracted from the interferometer measurement result. However, the midhigh frequency form errors were not subtracted due to the average effect of the capacitive sensor.

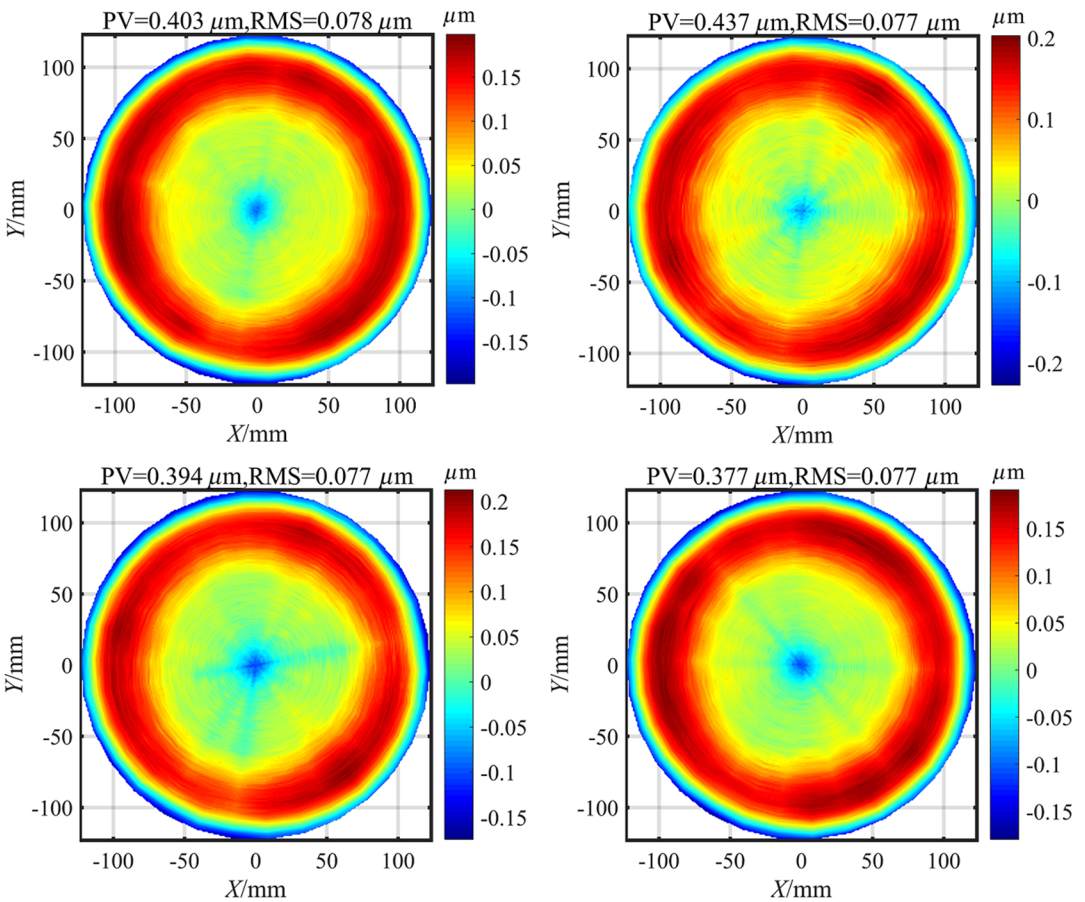

Fig. 13 Four successive measurement results of the mirror with 630.75-mm curvature radius.

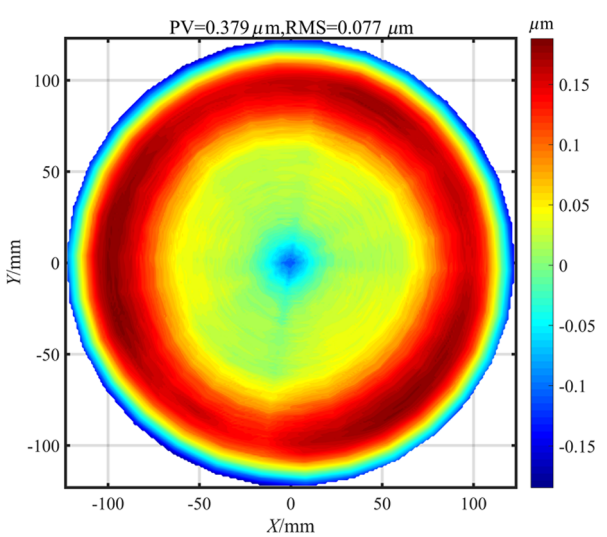

Fig. 14 The average result of the four measurement results.

4.2 *Verification of Compensation Cut*

After the initial cut, the surface form error of the mirror with 12.337-m curvature radius was measured using the proposed on-machine measurement system. The measured aperture was 276 mm, 92% of full aperture. The rotational speed of the spindle was set to 20 rpm and the sensor sampling frequency was set to 50 Hz. The angle-increment was 12 degree and the X-direction feedrate was 1.5 mm per revolution. The total measurement time of the mirror surface is <5 min.

A distribution map of the surface form error after the initial cut is shown in Fig. 18, and it can be seen that the error at the center region was similar to the shape of a mountain peak. Upon analysis, the form error at the center was caused by the X-direction decentering error of the diamond tool.[13] Note that the initial measurement form error was 0.969 μm in PV value, and was corrected to 0.971 μm after the linearity correction provided by the end-point reference calibration method, as shown in Fig. 9.

A new tool path was calculated by subtracting the measured form error from the theoretical surface form, and a compensation cut was performed using the new tool path. The form error after the compensation cut is shown in Fig. 19, and it can be seen that the peak at the center disappeared, although three raised regions appeared that were evenly distributed around the circumference. This is due to the fact that the mirror was mounted on the spindle using a three-point clamping method at the edge, as shown in Fig. 12. Upon analysis, the three raised regions correspond to the intervals between the tightening positions of the screws along the circumference where little material was removed due to the elastic deformation under the thrust cutting force. This indicates that the method of clamping the workpiece is one of the dominant factors affecting the surface form error when using diamond-cutting to shape large-diameter aluminum workpieces.

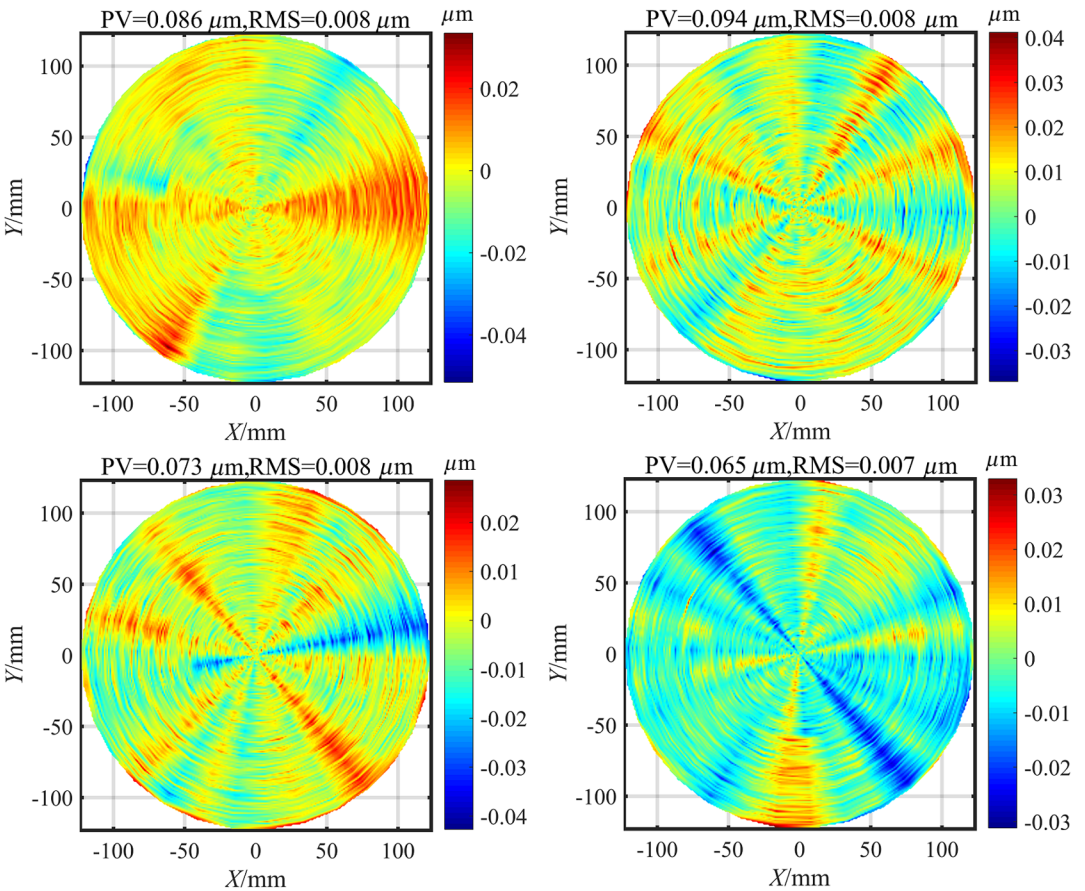

Fig. 15 Subtractions of measurement results to average result, corresponding to arrangement order in Fig. 13.

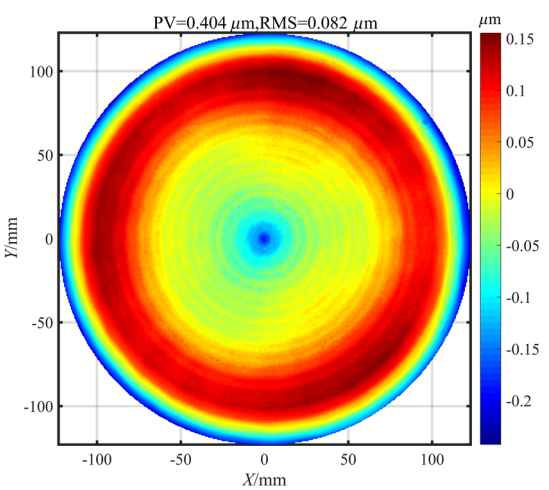

Fig. 16 Interferometer measurement result within 246-mm aperture.

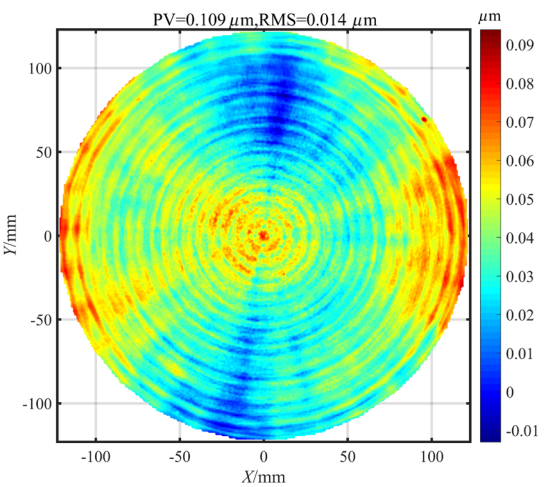

Fig. 17 Direct subtraction of the average result to the interferometer measurement result within the same aperture.

As shown in Fig. 19, the form error after a single compensation cut was a PV 254 nm and an RMS of 52 nm, which is better than $\lambda/10$ ($\lambda = 632.8$ nm). The convergence rate of the compensation was 73.8% and 70.3% for the PV and RMS, respectively. This demonstrates that the compensation process is very efficient, which contributes to a reduction in the cutting time thereby reducing the tool wear and decreasing the cost of the SPDT process.

4.3 *Measurement at High-Speed Rotation*

Figure 20 shows the cross-sectional profiles that pass through the center of the mirror with 12.337-m curvature radius at a spindle rotational speed of 1000 rpm, which is the same as that used in the experiment. In this case, the sampling frequency of the data acquisition unit was set to 1 kHz. In Fig. 20(a), the measurement sensor was triggered to record

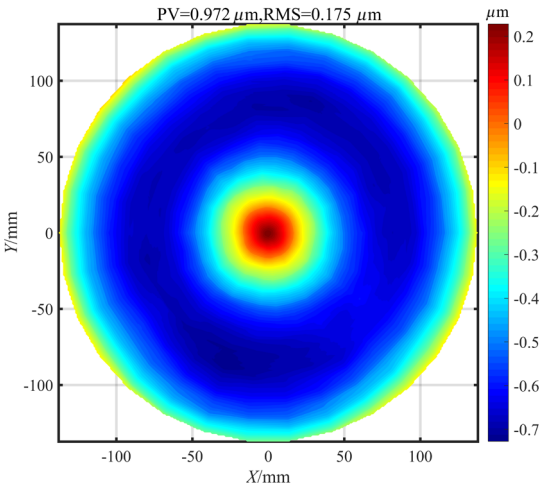

Fig. 18 Distribution map of the surface error after the initial cut.

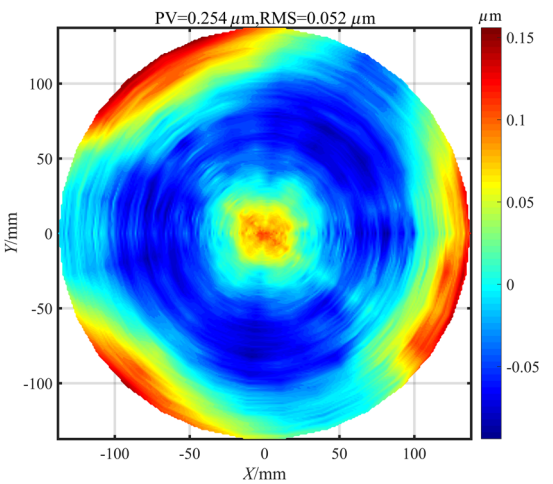

Fig. 19 Distribution map of the surface error after the compensation cut.

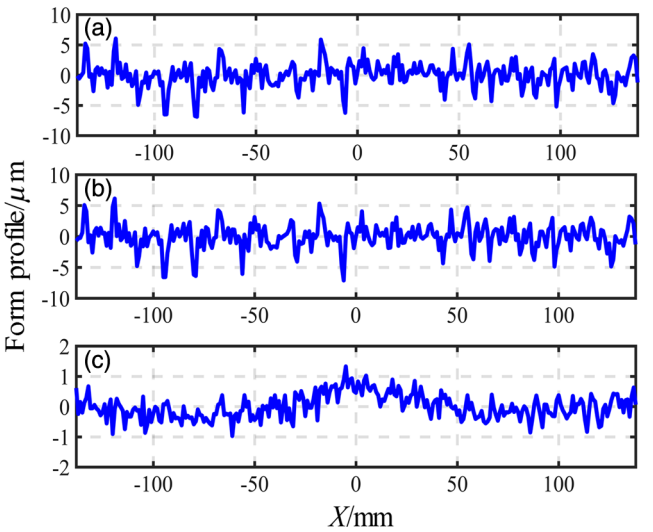

Fig. 20 Cross-sectional profiles of a one diameter scan at a spindle rotational speed of 1000 rpm (a) the measurement sensor readout, (b) the reference sensor readout, and (c) the data obtained after subtracting the data in (b) from that in (a).

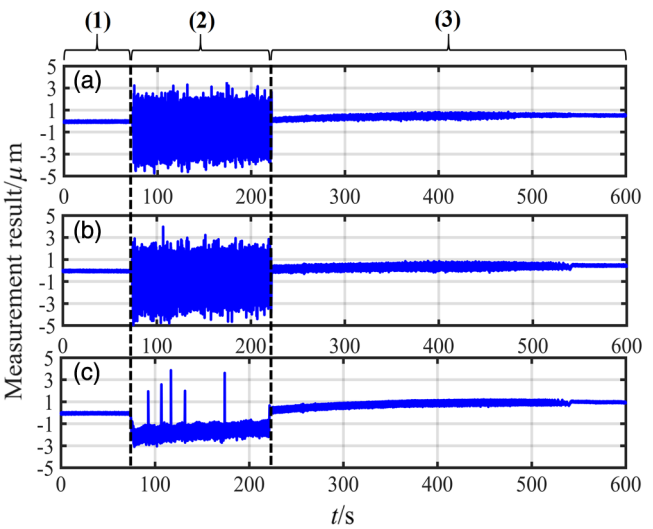

Fig. 21 Fixed-point measurement results at a rotation speed of 1000 rpm (a) the measurement sensor, (b) the reference sensor, and (c) the corrected data from the readouts of the two sensors.

the data for only one fixed diameter, whereas in Fig. 20(b) the reference sensor was triggered to record the data for only one fixed point. Both Figs. 20(a) and 20(b) show that the PV value of the noise level was about 10 μm. Data in Fig. 20(c) were obtained by subtracting the data in Fig. 20(b) from that in Fig. 20(a). After subtraction, the amplitude of the noise was decreased by an order of magnitude of about 1 μm.

To investigate the relationship between the generated noise and the spindle rotation speed, the performance of the capacitive sensors during spindle acceleration and deceleration was investigated. Under high-speed rotational conditions, the two sensors were simultaneously triggered to measure their own fixed points on the surface of the mirror with 12.337-m curvature radius. The investigation was performed in three steps, as shown in Fig. 21. In step (1), the spindle was stationary. In step (2), the spindle was accelerated from the stationary state to 1000 rpm, and then the speed was maintained for about 2 min. Finally, in step (3), the spindle was allowed to decelerate freely without any electric drive force. As shown in Fig. 21, the readouts of the two sensors were steady in step (1) and exhibited low-level white noise at the 1-kHz sampling frequency. In step (2), the readouts of both sensors were chaotic. In step (3), the level of the noise in the measurement results was lower, although it was still larger than that in step (1). Based on the above discussion, it was determined that the chaotic noise in step (2) was primarily induced by the electric drive rotating the spindle. Even though there was no drive electricity in step (3), it was assumed that the decelerating spindle introduced secondary noise due to electromagnetic induction, which caused the potential of the target surface to change.

In Fig. 21(c), drive electricity was initially applied to the spindle to move it back by about 2 μm before maintaining that position. Then, the electricity was removed at the end of step (2) and the spindle returned to the starting position. The PV value of the noise level in step (2), as shown in Fig. 21(c),

was about 2 μm, which is 66% less than the noise level of 6 μm in Figs. 21(a) and 21(b).

The above investigation shows that the noise level of the corrected data under high-speed rotation was significantly reduced by the reference sensor correction. To precisely measure the form error, a combination of a lower spindle rotational speed and low sampling frequency was indispensable under existing conditions to introduce much less noise into the measurement results. Nevertheless, the fact that <5 min were required for the measurement is valuable in view of 92% of the 300-mm full aperture. In addition, other advantages of the double sensor correction method can be applied elsewhere, such as in a spindle diagnosis application.

5 Conclusions

A noncontact on-machine measurement system using capacitive displacement sensors was developed for use on an ultraprecision machine tool. A position-trigger method of measurement was devised so that form error measurement of the optical surface could be realized. Finally, a double-sensor measurement was proposed and shown to be successful in reducing the influence of the electric signal noise caused by the spindle rotation. To test the repeatability and accuracy of the measurement method, a 93.9% of full aperture measurement of a spherical aluminum mirror with 262-mm diameter and 630.75-mm curvature radius was carried out four times continuously and then compared with the interferometer measurement result. The obtained repeatability was 80 nm in PV and 8 nm in RMS, whereas the achieved accuracy was 109 nm in PV and 14 nm in RMS. A 92% of full aperture measurement of a spherical aluminum mirror with a diameter of 300 mm was carried out, and the complete measurement of the form error required only 5 min. The obtained form error was then successfully used to modify the cutting tool path for the compensation cut. After a single compensation cut, the measured form error was reduced to 254 nm in PV and 52 nm in RMS, and the convergence rate of the measured form error was sufficiently high (up to 73.8% and 70.3% in PV and RMS, respectively), which is of great importance in reducing compensation-cut times and ensuring that diamond turning is deterministic.

Acknowledgments

The present work was partially supported by the National Nature Science Foundation of China (Grant Nos. 51775531 and 51305422), and the Youth Innovation Promotion Association, CAS (Grant No. 2014197). The authors declare no conflicts of interest.

References

1. L. Wamboldt et al., "An ultra-low surface finish process for 6061-Al mirrors," *Proc. SPIE* **9451**, 94511X (2015).
2. J. Yan et al., "Mechanism for material removal in diamond turning of reaction-bonded silicon carbide," *Int. J. Mach. Tools Manuf.* **49**, 366–374 (2009).
3. A. M. Patel et al., "Update on Tinsley visible quality (VQ) aluminum optics," *Proc. SPIE* **8353**, 83532C (2012).
4. S. Ralf et al., "Metal mirrors with excellent figure and roughness," *Proc. SPIE* **7102**, 71020C (2008).
5. M. Beier et al., "Fabrication of high precision metallic freeform mirrors with magnetorheological finishing (MRF)," *Proc. SPIE* **8884**, 88840S (2013).
6. J. P. Schaefer, "Advanced metal mirror processing for tactical ISR systems," *Proc. SPIE* **8713**, 871306 (2013).
7. S. Risse et al., "Novel TMA telescope based on ultra precise metal mirrors," *Proc. SPIE* **7010**, 701016 (2008).
8. D. Vukobratovicha and J. P. Schaefer, "Large stable aluminum optics for aerospace applications," *Proc. SPIE* **8125**, 81250T (2011).
9. L. Xiong et al., "Swing arm profilometer: high accuracy testing for large reaction bonded silicon carbide optics with a capacitive probe," *Opt. Eng.* **56**(8), 084101 (2017).
10. Micro-Epsilon Messtechnik GmbH & Co.KG, Instruction Manual capaNCDT 6500, "Capacitive displacement sensors and systems," http://www.microepsilon.com/download/products/cat--capaNCDT--en.pdf.
11. International Organization for Standardization, "Test code for machine tools—Part 1: geometric accuracy of machines operating under no-load or quasi-static conditions," International Standard ISO 230-1:2012(E).
12. R. Stefan et al., "Light weight structural element," EP1480005B1 (2004).
13. R. C. Juergens et al., "Simulation of single point diamond turning fabrication process errors," *Proc. SPIE* **5174**, 95 (2003).

Xingchang Li received his BS degree in electronic information engineering and his MS degree in optics from Jilin University in 2012 and 2015, respectively. Currently, he is a PhD student at CIOMP (Changchun Institute of Optics, Fine Mechanics and Physics, Chinese Academy of Sciences). He is working on single-point diamond turning (SPDT) of optics. His research interests include on-machine measurement and compensation in SPDT process.

Zhiyu Zhang received his BA and MS degrees from Jilin University and his PhD from Tohoku University. He is an associate professor of CIOMP. His research interest is set as optical fabrication by ultraprecision machining and laser direct writing. He has been working for more than 10 years on diamond turning of optics such as silicon, germanium, silicon carbide, aluminum, and aluminum-based composites.

Haifei Hu received his BA degree from Huazhong University of Science and Technology, his MS degree from Dalian University of Technology, and currently is a PhD student in Jilin University. He is an assistant professor of CIOMP. His research focuses on precise supporting system for *in-situ* testing optical elements and FEA simulation of optical fabrication process. He has been working for more than 7 years on optomechanical structure design, simulation, testing, and optimization.

Yingjie Li received his BA in mechanics from Jilin University, and his MS and PhD degrees in mechanics from Harbin Institute of Technology. He is an assistant professor of CIOMP. His research interest is set as optical grinding of silicon carbide large aperture mirror.

Ling Xiong received her BS degree in optics from Northwestern Polytechnical University in 2012 and her PhD at CIOMP (Changchun Institute of Optics, Fine Mechanics and Physics, Chinese Academy of Sciences) in 2017. She is working on optical testing for large-diameter optic segments. Her research interests include swing arm profilometer tests.

Xuejun Zhang received his BA degree from Jilin University of Technology in 1992, and his MS and PhD degrees in CIOMP. He is a professor and PhD adviser at CIOMP, where he is also director of the Key Laboratory of Optical System Advanced Manufacturing Technology. His interest is advanced optical system manufacturing.

Jiwang Yan is a professor of mechanical engineering at Keio University, Japan, leading the Laboratory for Precision Machining and Nano Processing. His research interests include ultraprecision machining, micro/nanomanufacturing, material processing, and optical fabrication. He has been working for more than 20 years on ultraprecision machining of hard and brittle materials and developed a series of novel fabrication processes.